Available online at www.sciencedirect.com
ScienceDirect
Journal of Nuclear Materials 372 (2008) 36–44
journal of nuclear materials
www.elsevier.com/locate/jnucmat

Optical anisotropy measurements of TRISO nuclear fuel particle cross-sections: The method

G.E. Jellison Jr. *, J.D. Hunn

Materials Science and Technology Division, Oak Ridge National Laboratory, Oak Ridge, TN 37831-6030, United States

Received 14 November 2006; accepted 6 February 2007

Abstract

The analysis of two-modulator generalized ellipsometry microscope (2-MGEM) data to extract information on the optical anisotropy of coated particle fuel layers is discussed. Using a high resolution modification to the 2-MGEM, it is possible to obtain generalized ellipsometry images of coating layer cross-sections with a pixel size of 2.5 μm and an optical resolution of ~4 μm. The most important parameter that can be extracted from these ellipsometry images is the diattenuation, which can be directly related to the optical anisotropy factor (OAF or OPTAF) used in previous characterization studies of tristructural isotropic (TRISO) coated particles. Because high resolution images can be obtained, the data for each coating layer contains >6000 points, allowing considerable statistical analysis. This analysis has revealed that the diattenuation of the inner pyrocarbon (IPyC) and outer pyrocarbon (OPyC) coatings varies significantly throughout the layer. The 2-MGEM data can also be used to determine the principal axis angle of the pyrocarbon layers, which is nearly perpendicular to the TRISO radius (i.e., growth direction) and corresponds to the average orientation of the graphene planes.

PACS: 28.41.Bm; 42.25.Ja; 78.67.−n

1. Introduction

Tristructual isotropic (TRISO) coated particle fuel consists of a spherical kernel and four layers. The kernel is the nuclear fuel, typically uranium oxide or uranium oxide plus uranium carbide, where the uranium is enriched in the U^{235} isotope. The kernel is sealed within the following concentric layers through fluidized bed chemical vapor deposition (CVD): a porous graphite/amorphous carbon layer (buffer), a denser graphite/amorphous carbon layer (inner pyrolytic carbon or IPyC), a layer of polycrystalline silicon carbide (SiC), and an outer, dense graphite/amorphous carbon layer (outer pyrolytic carbon or OPyC). Each of these layers performs a specific function: the SiC is the primary fission product retention barrier, the buffer attenuates fission recoils and provides space for kernel expansion and gas emission, the IPyC acts as a secondary retention barrier and protects the kernel during SiC deposition, and the OPyC acts as a secondary retention barrier and provides an interface for compacting.

The buffer, IPyC, and OPyC layers consist mostly of nanocrystalline graphite with some amorphous carbon. Crystallographically, graphite is a layered hexagonal structure (point group D_{6h} or C_{6v}) [1]. Within the graphene planes, the carbon atoms are 3-coordinated and the bonds are strong; intra-plane bonding is very weak. It is well-known that pyrolytic graphite can be crystallographically isotropic on the μm scale, where there is no preferential orientation of the graphene planes, or have varying degrees of crystallographic anisotropy (preferential orientation), depending on the fabrication procedure [2,3]. For the IPyC and the OPyC of TRISO coated particles, it is known [4] that too much preferential orientation leads to anisotropic dimensional changes of the IPyC or OPyC during irradiation, possibly resulting in failure of the SiC layer.

The quantification of this preferential orientation of the graphite nanoparticles in the IPyC and OPyC in TRISO

* Corresponding author. Tel.: +1 865 576 7309; fax: +1 865 574 4143.
E-mail address: jellisongejr@ornl.gov (G.E. Jellison Jr.).

0022-3115/$ - see front matter © 2007 Elsevier B.V. All rights reserved.
doi:10.1016/j.jnucmat.2007.02.008

particles is complicated by the fact that the thickness of the three outer layers is 20–40 μm. It is possible to measure this by micro-beam X-ray techniques [5], but this technique is slow, inaccurate, and requires a significant investment in measurement equipment.

The primary technique that has been used in the past is polarization-sensitive optical microscopy [6]. This technique takes advantage of the very large optical anisotropy of graphite for reflection of light polarized parallel to or perpendicular to the graphene layers [7–9]. If there is a preferential orientation of the graphite nanoparticles in a pyrocarbon layer, then there will be some difference in the polarization-sensitive reflectivity of the material, which can be observed under certain conditions.

The traditional technique to measure optical anisotropy of pyrocarbon layers in TRISO particles starts with the preparation of the samples, which are placed in an epoxy matrix and ground/polished down to expose a cross section of the particle. The TRISO particle cross-section is then examined using a polarization microscope, where the maximum and minimum reflectivities are found at the same spot on the sample. From this, it is possible to calculate the optical anisotropy factor (OAF or OPTAF):

$$\mathrm{OAF} = R_{\max}/R_{\min}, \tag{1}$$

where $R_{\max}$ ($R_{\min}$) is the maximum (minimum) reflectivity and ideally should correspond to the polarized light oriented parallel to (perpendicular to) the preferred orientation of the graphene planes. The light source can be either a laser, such as HeNe at 632.8 nm, or filtered white light, such as from a tungsten-halogen lamp. Some of the early instruments passed both the input and output beams through polarization filters, while others polarized only the input beam. As can be seen from Eq. (1), two parameters must be measured. This involves the rotation of the sample or the polarizers, or (in the case of Ref. [4]) the exchanging of two polarizers oriented at 90° with respect to one another. Another instrument used to measure OAF is the Stevens microellipsometer, where the polarization change results from the rotation of a 1/2 waveplate [10].

While a detailed analysis of earlier experiments is not possible because of the lack of details in the literature, several potential problems can be identified. All of these instruments have some problems with registration, in that the rotated/moved optic changes the position of the image in the microscope. In all cases, the measurements are made sequentially, so fluctuations in the light source could result in significant error. The wavelength of the probe light also was different for several of the earlier experiments, ignoring the wavelength dependence of the optical properties of the pyrocarbon. If a laser light source is used, then light coherency and speckle become problems. As a result, many of the earlier results were not consistent [11].

We have recently developed another technique to measure the optical anisotropy based on the principles of generalized ellipsometry [8,9,12–14]. This instrument is called the two-modulator generalized ellipsometry microscope (2-MGEM), and determines eight parameters at each point measured. The availability of so much additional data opens new opportunities for the understanding of optical anisotropy in the IPyC and OPyC layers of TRISO particles, but also necessitates a methodology for reducing the data. In this paper, we will present the data from a single TRISO cross section and discuss the analysis methodology that has been developed.

2. Description of the experiment and data presentation

The 2-MGEM is based on the two-modulator generalized ellipsometer (2-MGE) [13,14] and is described in detail in Ref. [12]. Briefly, the instrument is arranged as a reflection microscope with a single large-aperture objective acting as both the condensing lens and the objective. The input beam passes through the polarization state generator (PSG), which consists of a polarizer photoelastic modulator (PEM) pair placed before the objective. The reflected beam, after passing through the objective, passes through the polarization state analyzer (PSA), which also consists of a polarizer PEM pair. The two PEMs are operated at different frequencies (50 and 60 kHz in this case). The light intensity is detected as a function of time using a photomultiplier tube, which is then digitized at 0.5 μs/point. The light source is a mercury arc lamp, which is filtered at 577 nm (one of the primary emission lines of the mercury lamp). The intervening large-aperture objective does perturb the polarization measurement, but many of the effects can be calibrated out (see Ref. [12]). The optical resolution of the experiment is determined by the optical elements after the sample and the pinhole in front of the photomultiplier tube (PMT). The primary data discussed in this paper were collected using a 25 μm diameter pinhole, resulting in an optical resolution of ~4 μm; this compares to the standard resolution of this instrument, where the pinhole was 50 μm, resulting in an optical resolution of ~8 μm (see Refs. [8,12]). Alternatively, higher resolution may be obtained by replacing the condenser/objective lens with one with a shorter focal length.

The time-dependent intensity is a complicated function of time, but can be expressed as [13,14]

$$\begin{aligned}\mathrm{Intensity}(t) = {} & I_{\mathrm{dc}} + I_{\mathrm{X0}}\mathrm{X0} + I_{\mathrm{Y0}}\mathrm{Y0} + I_{\mathrm{X1}}\mathrm{X1} + I_{\mathrm{Y1}}\mathrm{Y1} \\ & + I_{\mathrm{X0X1}}\mathrm{X0}\ \mathrm{X1} + I_{\mathrm{X0Y1}}\mathrm{X0}\ \mathrm{Y1} \\ & + I_{\mathrm{Y0X1}}\mathrm{Y0}\ \mathrm{X1} + I_{\mathrm{Y0Y1}}\mathrm{Y0}\ \mathrm{Y1}. \end{aligned} \tag{2a}$$

The terms I_{dc}, I_{X0}, I_{Y0}, etc. are coefficients that multiply the basis functions:

$$\mathrm{X0} = \sin(A_0 \sin(\omega_0 t)); \quad \mathrm{Y0} = \cos(A_0 \sin(\omega_0 t)), \tag{2b and c}$$

$$\mathrm{X1} = \sin(A_1 \sin(\omega_1 t)); \quad \mathrm{Y1} = \cos(A_1 \sin(\omega_1 t)). \tag{2d and e}$$

The basis functions are not common Fourier basis functions, but rather sines and cosines of sines. The modulator amplitudes (A_0 and A_1) are measured in angular units

(usually radians) and the modulator frequencies are given by ω_0 and ω_1. The intensity is normalized to the dc level, and this is done both in hardware and software.

The coefficients of the basis functions are the measured quantities in the experiment, and are functions of the azimuthal orientation of the PSG and PSD. For the case where the PSG is oriented at 0° with respect to the measurement system and the PSA is oriented at 45°, then the eight coefficients are

$$I_{X0} = \mathrm{CD} \quad I_{X1} = -\mathrm{CD} \qquad \text{(3a and b)}$$

$$I_{Y0} = \sin(2\gamma)N \quad I_{Y1} = -\cos(2\gamma)N \qquad \text{(3c and d)}$$

$$I_{X0X1} = -C \quad I_{Y0X1} = -\cos(2\gamma)S \qquad \text{(3e and f)}$$

$$I_{X0Y1} = \sin(2\gamma)S \quad I_{Y0Y1} = \cos(2\gamma)\sin(2\gamma)(1+C). \qquad \text{(3g and h)}$$

For TRISO particles, the two most important parameters are the diattenuation N and the direction of the principal axis γ, which is referenced to the measurement system. Therefore, it is critical for the measurement system to determine the parameters I_{Y0} and I_{Y1} as accurately as possible. For other applications, the retardation δ and the circular diattenuation CD are important. The retardation is determined from the S and C parameters: $S = (1 - N^2)^{1/2}\sin(\delta)$ and $C = (1-N^2)^{1/2}\cos(\delta)$, which are determined from I_{X0X1}, I_{X0Y1}, and I_{Y0X1}. Obviously, N, S, and C are not independent, since $N^2 + S^2 + C^2 = 1$. However, if the sample depolarizes the light beam, then the sum $N^2 + S^2 + C^2 = \beta^2 < 1$.

The sample examined for this work was a TRISO coated particle from a fuel compact prepared by Oak Ridge National Laboratory for irradiation testing in the Advanced Test Reactor at Idaho National Laboratory as part of the Department of Energy's Advanced Gas Reactor Fuel Qualification and Development program. This particle was coated with a set of baseline conditions designed to produce coatings with optimal predicted performance based on the existing database for coated-particle fuel. The particle was encased in an epoxy matrix and ground/polished to expose a cross-section of the particle close to the midplane. The polishing was performed using progressively finer diamond compounds on a rotary platen. Because of the different mechanical properties of the SiC and pyrocarbon layers, it is important to balance the reduction of average surface roughness against the loss of surface flatness. Excessive polishing tends to result in a tapering of the pyrocarbon layers away from the harder SiC layer. Both surface roughness and loss of flatness result in a reduction in the signal-to-noise ratio for the measurement due to optical scatter (reflected light that does not go through the pinhole into the PMT). In a 2-MGEM measurement which is based on relative amplitudes, optical scatter does not result in systematic measurement error, as it would for a polarimeter measurement of OAF which is based on the difference in intensity between the incident and reflected light, but lower light throughput does result in lower signal-to-noise ratio.

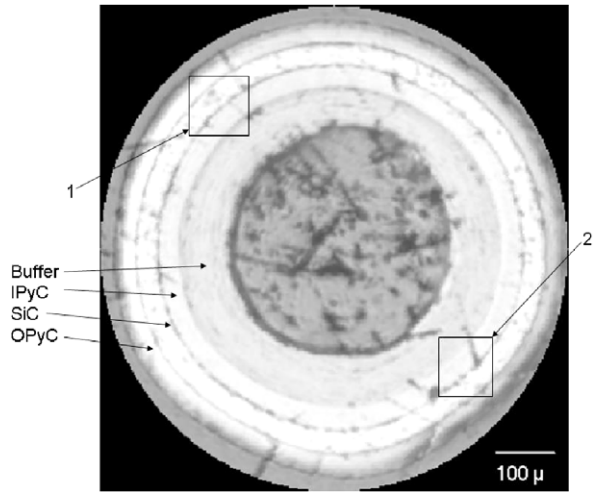

Fig. 1. Intensity map of a TRISO coated particle cross section. The greyscale is logarithmic, where black corresponds to an intensity that is ~1/300 that of white. The kernel of the particle has been removed and the void back-filled with epoxy. The buffer, IPyC, SiC, and OPyC layers are clearly imaged in the figure, and two regions are selected that are shown in more detail in Fig. 3.

A series of 2-MGEM measurements are made sequentially by rastering the sample on a two axis computer-controlled stage such that the light intensity and the eight parameters with associated errors (see Eqs. (2) and (3)) are determined at each x–y point in the scanned array. This gives a 2-MGEM data array of the surface, from which can be extracted images of the various parameters calculated using the equations above. The resolution of these images is determined by the imaged spot size and the step size of the array. For the example discussed in this paper, the step size was 2.5 μm and 10 measurements were taken at each step to enable us to determine an average value and associated error. An intensity image of the particle is shown in Fig. 1, which consists of $281 \times 276 = 77\,556$ points (particle diameter ~800 μm). Fig. 2 shows images of the I_{Y0} and I_{Y1} coefficients along with the associated derived images of the diattenuation and fast axis, described in the next section.

The image of the TRISO coated particle shown in Fig. 2 shows clearly the separation between the four layers, but also shows residual scratches left from the polishing. As discussed above, this surface roughness was not removed because additional polishing would have resulted in greater signal loss due to loss of flatness.

3. Analysis of the data

The most important parameter for TRISO particle characterization is the optical diattenuation N. For optically anisotropic materials, the reflectivity will depend on the polarization state of the light beam. The diattenuation is defined as

$$N = \frac{R_{\max} - R_{\min}}{R_{\max} + R_{\min}}, \qquad (4)$$

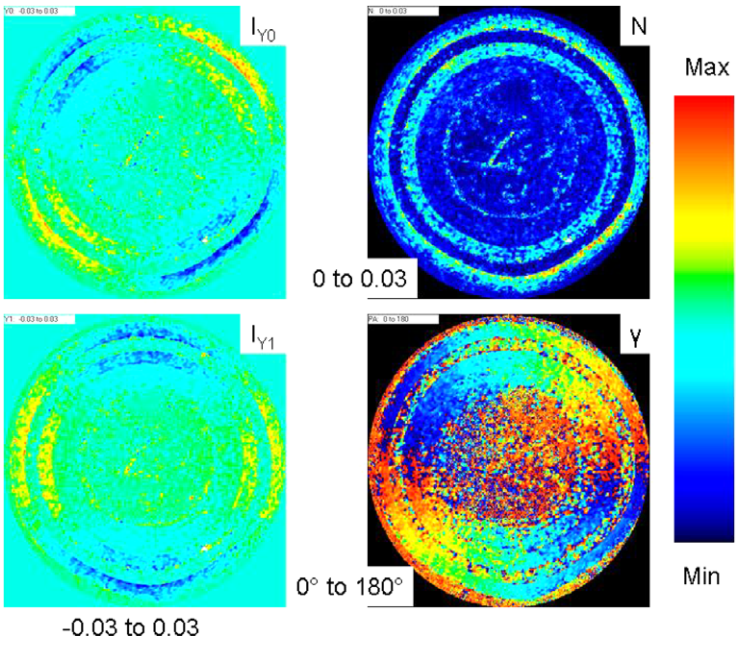

Fig. 2. The raw data (left) for quantities I_{Y0} and I_{Y1}, from which the diattenuation N and direction of the principal axis angle γ (right center) are determined. The linear color scale is shown at the far right.

where R_{max} (R_{min}) is the maximum (minimum) reflectivity for orthogonal polarization states of the incident light. Obviously, the diattenuation is then directly related to the optical anisotropy factor OAF (see Eq. (1)):

$$\mathrm{OAF} = \frac{1+N}{1-N} \sim 1 + 2N, \tag{5}$$

where the first-order Taylor expansion is used to obtain the second expression. Clearly, these expressions represent an integration over the sampled region (~4 μm in this case).

For pyrolytic carbon, the optical anisotropy originates from the preferential orientation of nanocrystalline graphite. Since the sampled region is considerably larger than the individual graphite nanocrystals, the optical response will be an integration over all the nanoparticles within the 4 μm sampled regions. If the graphene planes of the individual graphite nanoparticles are preferentially oriented, then the reflectivity will be polarization-sensitive (that is, optically anisotropic), while a totally random collection of graphite particles will result in no observable optical anisotropy after integration over the 4 μm sampled region.

3.1. Normalization

The 2-MGEM is designed to operate at near-normal incidence, where the angle of incidence is 3–5°. The minor deviation from normal incidence results in a small residual diattenuation from the non-zero angle of incidence [12]. As a result, the two diattenuation-sensitive parameters (I_{Y0} and I_{Y1}) experience a small bias in their values, which must be subtracted out to get the most accurate diattenuation measurements.

For TRISO particles, any real preferred orientation is expected to be related to the growth direction (along the radius of the particle). Therefore, in the image of the particle, the preferred orientation will rotate 360° as one goes around the particle. In contrast, the bias for a non-zero angle of incidence will be dependent only on the angle of incidence and the complex refractive index of the material and will not be dependent upon the growth direction. This suggests a technique for compensating for the angle-of-incidence effect: A large donut-like region of the buffer is selected and the averages of the measured values of I_{Y0} and I_{Y1} (as well as I_{X0}, I_{X1}, I_{X0Y1}, I_{Y0X1}, and I_{Y0Y1}) are calculated. The data for the entire image are then normalized for this small offset by subtracting off the average. The buffer region is selected because it is expected that its diattenuation will be considerably smaller than the diattenuation of the IPyC or the OPyC, but its complex refractive index will be similar to that of the IPyC and OPyC layers. The SiC layer may also be a candidate for this procedure, but the refractive index of the SiC may be considerably different from that of the pyrocarbon layers.

3.2. Diattenuation N

The diattenuation and the direction of the principal axis can be determined from only the I_{Y0} and the I_{Y1} terms in Eqs. (3c) and (3d), which are shown in Fig. 2. The diattenuation and the direction of the fast axis are given by

$$N = \sqrt{I_{Y0}^2 + I_{Y1}^2}, \quad \text{and} \tag{6a}$$

$$\tan(2\gamma) = -\frac{I_{Y0}}{I_{Y1}}, \tag{6b}$$

which are also shown in Fig. 2. Clearly, the determination of γ must use the sign values of I_{Y0} and I_{Y1} to allow a determination from 0° to 180°. (Note that we have simplified the

definition of diattenuation from that used in Ref. [12], where we also considered the sign of N.) Smaller values of N will necessarily result in more inaccurate determinations of γ, where in the limit of $N = 0$, γ becomes indeterminate.

To get a better picture of the accuracy and the level of detail that the 2-MGEM measurement gives, two sections of the data in Fig. 2 are enlarged in Fig. 3. In this presentation of the data, the direction of the principal axis angle γ is shown graphically by a separate line segment for each data point in the image array, which also corresponds to the preferential orientation of the graphene planes. As can be seen from the data presented in both Figs. 2 and 3, the diattenuations in both the SiC and Buffer layers are very small. The normalization procedure will correct for a uniform bias of I_{Y0} and I_{Y1}, making even small values of diattenuation, as long as they are greater than the average error, significant. The small value of the diattenuation in the SiC layer is not forced by the normalization, but is obviously quite small, giving us a consistency check on the normalization procedure. Both the IPyC and OPyC layers contain regions of relatively high diattenuation, but also regions of much lower diattenuation. In pixels where the diattenuation is high, the direction of the principal axis γ is nearly perpendicular to the radius line from the center of the TRISO particle (i.e., the growth direction), while regions of lower diattenuation do not have such a well-defined direction for γ. It is clearly evident from the data depicted in Figs. 2 and 3, that the diattenuations of the IPyC and OPyC layers are not constant throughout the layer. For this reason, it is not sufficient to obtain an average diattenuation value for each layer based on only a few measured regions. A more sophisticated, statistically oriented data analysis method, such as that described in Section 3.4, is required.

To get a quantitative measure of the quality of the diattenuation measurement, we also determine the polarization factor β, shown in Fig. 4 (significant depolarization is indicated when β is less than ~0.99). For the example shown in Fig. 4, the IPyC and the SiC show a consistent value of β close to unity, apart from obvious scratches and pits (also evident in the intensity map in Fig. 1) and a ring on both sides of the SiC layer where there was excessive chipping of the SiC edge. On the other hand, the buffer layer and the OPyC show much more variation in the polarization factor, indicating the greater surface roughness of these layers. Surface defects such as scratches, pits, and pores, often result in regions of significant depolarization. The OPyC layer often shows more depolarization due to the difficulty in obtaining a polished surface without rounding.

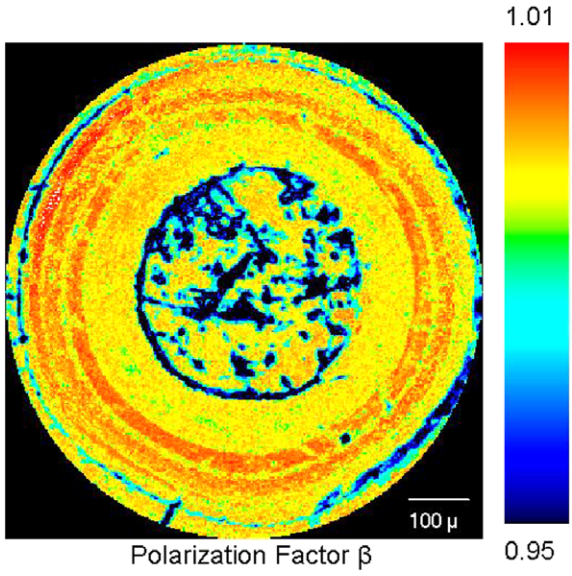

Fig. 4. The polarization factor β for the data shown in Figs. 1–3.

The error of the diattenuation can also be calculated by propagating the individual errors of I_{Y0} and I_{Y1} using Eq. (6). This is important because the measured diattenuation

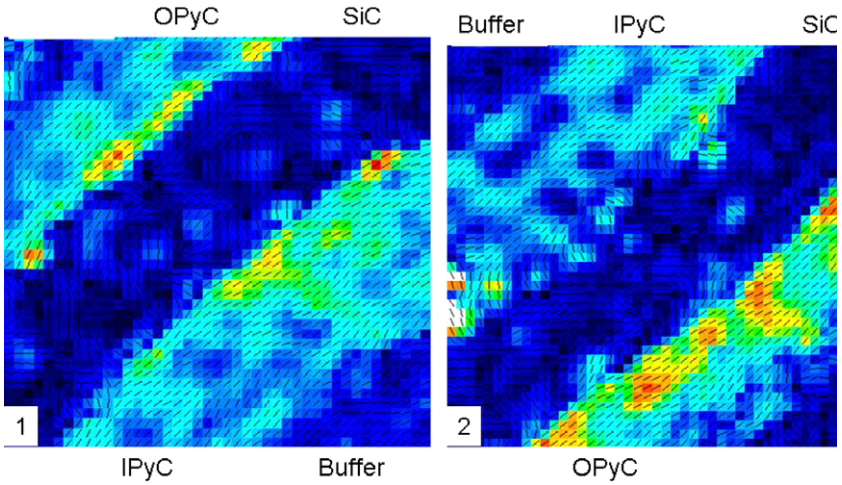

Fig. 3. Details of the diattenuation N of regions 1 and 2 of Fig. 1, using the color scale shown in Fig. 2, where the minimum color (black) corresponds to $N = 0$, and the maximum color (red) corresponds to $N = 0.035$. The direction of the principal axis for each pixel is depicted by a superimposed line. Each pixel measures 2.5×2.5 μm.

N as determined from Eq. (6) will always be biased toward a positive quantity, even though the true value is zero. Therefore, a measured value of N that is less than approximately twice the error cannot be considered different from zero.

3.3. Measurement of the relative direction of the principal axis

It can be clearly seen from Figs. 2 and 3 that the direction of the principal axis in the IPyC and OPyC lies nearly perpendicular to the radial line of the particle, which corresponds to the growth direction. Similar measurements on highly oriented pyrolytic graphite (HOPG) discussed in Refs. [8,9] show that this preferential orientation of the principle axis in graphite is perpendicular to the c-axis and is therefore parallel to the graphene planes. This orientation is what is expected for carbon deposited directly on the growth surface.

To quantify the orientation of the principal axis, we define the relative principal axis angle γ_r, which is the principal axis angle γ with respect to the radial vector of the TRISO particle. If the particle is spherical, then perfect alignment results in $\gamma_r = 90°$. If the fraction of the pyrocarbon layer producing the optical diattenuation is well-organized, then γ_r will be close to 90°, and the standard deviation of γ_r [SD(γ_r)] for a collection of points within the layer will be small. If the layer is not well organized, γ_r may still be close to 90°, but the SD(γ_r) for a collection of points within the layer will be large. (A similar increase in SD(γ_r) can be expected from the non-spherical nature of real TRISO particles.) It can be shown that a totally uncorrelated collection of relative principal axis angles (corresponding to a random collection) will have a SD(γ_r) = 52.0°. Therefore, the SD(γ_r) becomes a quantitative measure of the degree of organization within the pyrocarbon layers: perfect organization in perfectly spherical particles results in SD(γ_r) = 0°, perfect disorganization results in SD(γ_r) = 52.0°. Obviously, care must be taken when a TRISO particle has a significantly non-spherical shape, since this can also contribute to SD(γ_r).

3.4. Assignment of regions and histograms

While manual polarimeter measurements of OAF are time-consuming and therefore only a limited number of measurements are made on each layer, the 2-MGEM described in this paper is typically used to measure many thousands of points over the whole TRISO particle cross-section, and 1000–10 000 points within each pyrocarbon layer. This added capability dramatically improves the reliability and accuracy of the 2-MGEM measurements. After an array of points is measured over the entire particle cross section, the regions corresponding to each layer are identified in order to extract the data and perform statistical analysis on the values associated with each layer. This would be fairly easy if the particles were perfectly spherical, but this is often not the case. At this time, we use a semi-automated scheme to select most of the points associated with each individual layer in the image of the TRISO particle cross-section. This scheme involves performing the following steps to identify a region of interest for each layer using the intensity image shown in Fig. 1:

1. Select 8–12 points around each layer located near the center of that layer. Given the non-uniformity of the particles, this is best done by hand.
2. Convert these points to polar coordinates and sort the points by polar angle.
3. Perform a spline interpolation.
4. Select a width for the region of interest (usually 3–4% of the total image size for the buffer layer and 1–1.5% of the total image size for the IPyC, SiC and OPyC layers); this defines a region between two modified concentric circles, where all the points within the region lie within the selected layer.
5. Plot the two modified concentric circles on the intensity image (such as in Fig. 1) for a visual check that only points from the layer of interest are included.

In our analysis software, step 1 is performed by hand, while steps 2–5 are performed by the computer, after certain defining parameters are input. It is then possible to perform a number of statistical manipulations on the groups of data thus selected. This data analysis will be discussed in the next section.

4. Results and discussion

The histogram results are shown in Fig. 5 for the diattenuation N, in Fig. 6 for the relative direction of the principal axis γ_r, and in Fig. 7 for the polarization factor β of our sample particle. A statistical summary is shown in Table 1, where we have also included data taken from the same TRISO particle, but measured at a lower resolution (50 μm pinhole, resulting in an optical resolution of ~8 μm, with a pixel size of 5 × 5 μm).

The histograms of the diattenuation (Fig. 5) show the data most relevant to the performance of the TRISO particle. There is a small but observable diattenuation associated with the buffer and SiC layers. (Recall that a diattenuation near 0 cannot be measured accurately and will be biased toward a positive value.) The most significant diattenuation occurs in the OPyC and IPyC layers, and the distribution width is considerably larger than the average errors. This affirms the observation of non-uniform distributions of the diattenuation in these layers (see Figs. 2 and 3), discussed earlier. The advantage of the present analysis, however, is that now we can quantify this distribution.

The distribution of the direction of the relative principal axis angle γ_r, shown in Fig. 6, supports the conclusion that the OPyC and IPyC layers are better ordered than either the buffer or SiC layers. Both the buffer and SiC layers

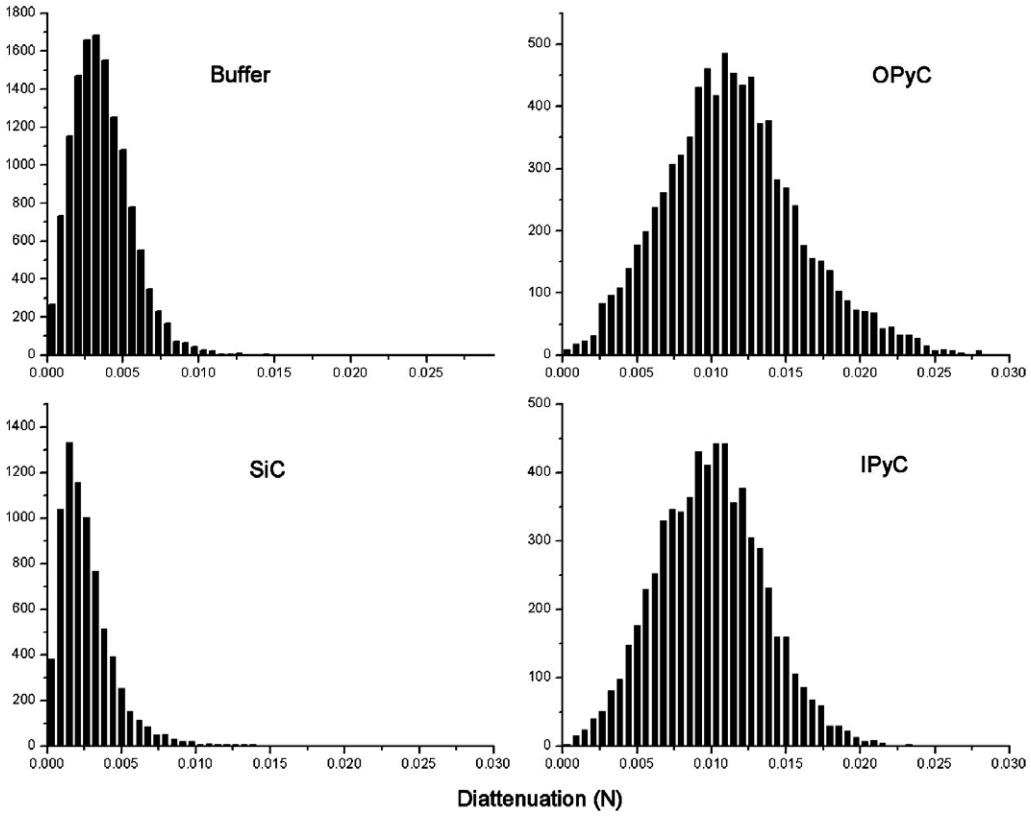

Fig. 5. Histograms of the diattenuation N for the four layers of the TRISO coated particle.

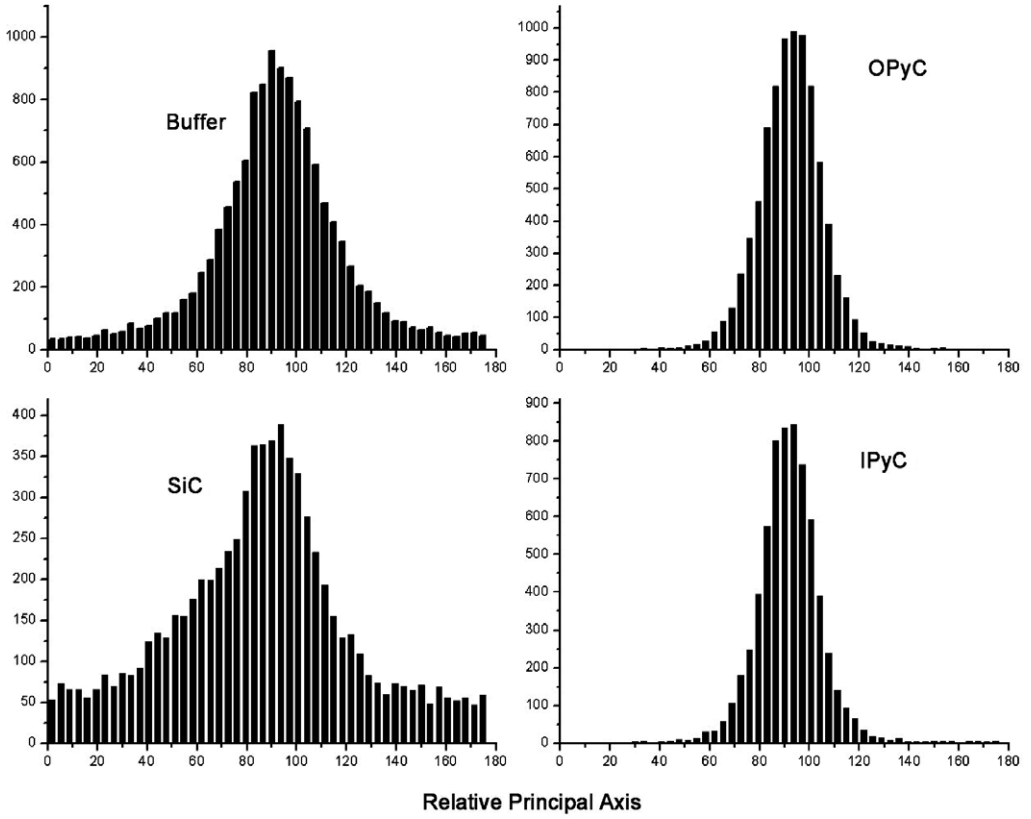

Fig. 6. Histograms of the principal axis angle relative to the center of the TRISO particle for the four layers of the TRISO particle.

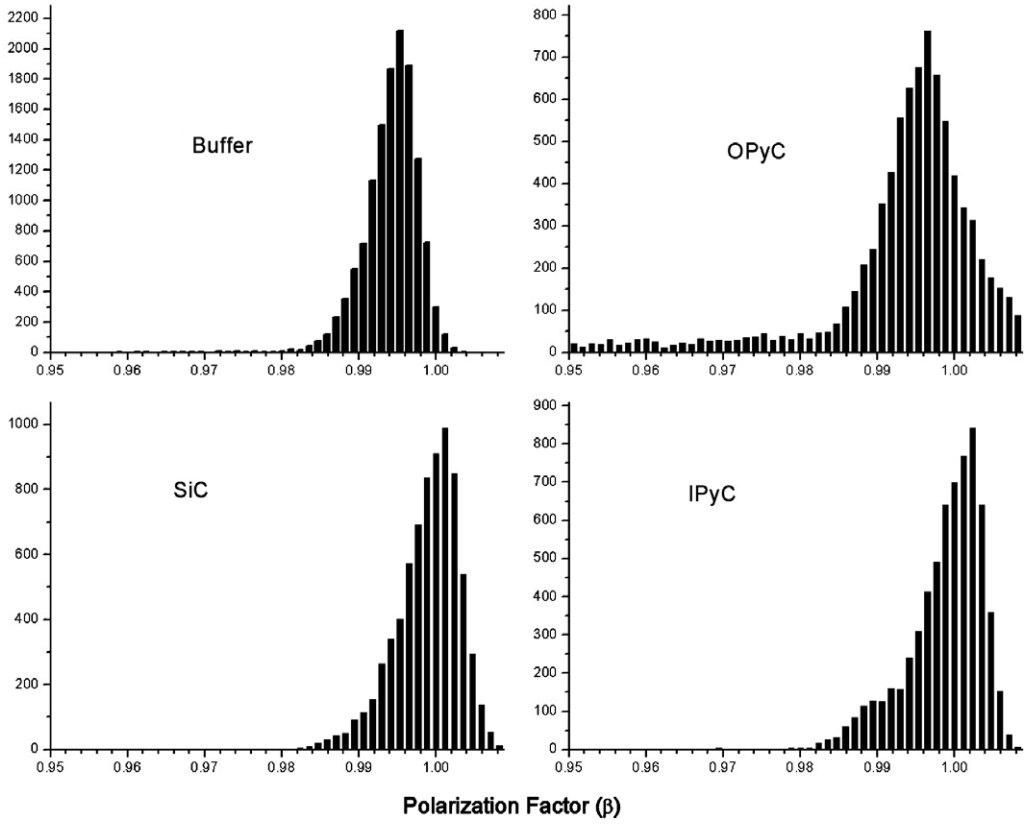

Fig. 7. Histograms of the polarization factor β for the 4 layers of the TRISO particle.

Table 1
Summary of the data obtained from the histograms shown in Figs. 5–7 and similar histograms for a lower resolution measurement

Parameter	Buffer	IPyC	SiC	OPyC
High resolution (25 μm pinhole, 2.5 μm/step)				
# points	13155	6554	7417	8296
$\langle N \rangle$	0.0036	0.0101	0.0027	0.0114
Std. dev.	0.0019	0.0061	0.0019	0.0046
Ave. err.	0.0007	0.0006	0.0005	0.0008
SD(γ_r)	28.0	13.8	37.5	13.5
Ave. pol. fact (β)	0.994	0.998	0.999	0.993
Low resolution (50 μm pinhole, 5 μm/step)				
# points	1966	1253	1408	1567
$\langle N \rangle$	0.0033	0.0097	0.0034	0.0121
Std. dev.	0.0017	0.0043	0.0018	0.0042
Ave. err.	0.0015	0.0013	0.0011	0.0015
SD(γ_r)	23.3	10.3	41.9	9.9
Ave. pol. fact s(β)	0.998	0.996	1.000	0.998

seem to be preferentially oriented, but the small value of the diattenuation in both layers leads to quite large errors in this quantity. The standard deviation of the relative principal angle (shown in Table 1), is a quantitative measure of the graphene plane ordering, which is a significant advantage over polarimeter measurements of OAF.

The origin of this diattenuation from the four layers of TRISO coated fuel is still not fully understood, but we can make some general observations. In the SiC layer, the diattenuation is very small, but it is larger than the average error. This indicates that there is some preferential orientation in this layer. The SiC layer consists mostly of cubic β-SiC, although there may be a small amount of hexagonal α-SiC [15]. Even though the cubic SiC is preferentially oriented during deposition, this does not result in any observable diattenuation because cubic SiC is not optically anisotropic. However, the SiC layer is significantly strained when particles are cooled down from the deposition temperature, and this strain could result in the observed diattenuation.

The carbon-based layers (Buffer, IPyC and OPyC) consist of quasi-spherical graphite particles (<1μm in diameter), probably nucleated in the gas phase and then deposited with additional graphite-like material deposited directly on the growth surface [16]. Since the optical resolution is less than the graphite particle size, no net diattenuation would result from the spherical graphite particles, even though each sphere is highly oriented. However, the material deposited directly on the growth surface could result in the preferential orientation of graphite nanoparticles perpendicular to the growth direction. Since the buffer layer is grown much faster than either the IPyC or the OPyC layers (~20 μm/min versus ~4–5 μm/min) and with a different gas composition, it is not unreasonable to expect a greater preferential orientation of the graphite nanoparticles in the slower grown layers. In fact, it has been shown [17] that the diattenuation in the IPyC and OPyC layers

increases with decreasing deposition rate and decreasing porosity.

The histograms of the polarization factor β, shown in Fig. 7 allow us to quantify the general conclusions concerning the data presented in Fig. 4. The IPyC and SiC layers show a very strong peak in this factor near one, indicating no observable depolarization. However, both distributions show a tail extending significantly below one; this is due to depolarization caused by surface defects, such as scratches and pits (see Figs. 1 and 4). The average of β for the buffer layer is 0.994, which indicates that there is a small amount of depolarization from this layer; this is probably due to the very porous nature of this layer. The greatest amount of depolarization is found in the OPyC (average $\beta = 0.993$); this is likely due to the difficulty of getting a good polish on this layer. (The OPyC lies between the hard SiC layer and the epoxy, making it very difficult to get a polished surface without excessive loss of flatness.)

It is instructive to compare the results from the high resolution measurement discussed so far with results obtained at the lower resolution (see Table 1). There are small differences in the average diattenuation, but the differences are not significant compared to the relative errors. The largest difference between the two data sets lies in the standard deviation of the diattenuation distribution of the IPyC layer, which is considerably larger for the high resolution measurement than for the low resolution measurement. Furthermore, the relative principal axis angle distribution standard deviation SD(γ_r) is also much larger for the high resolution measurement than for the low resolution measurement. Both observations can be understood from the non-uniformity of the diattenuation in these layers. With lower resolution, the 2-MGEM integrates over a larger area than does the higher resolution measurements, averaging out some of the variation.

5. Conclusions

We have shown that the two-modulator generalized ellipsometer (2-MGEM) can be used to generate images of the optical diattenuation and direction of the principal axis of TRISO coated-particle cross sections. Although these data are related to the earlier OAF measurements, the thoroughness of the analysis allows for the creation of histograms of data for each of the layers in TRISO coated particles, giving a far more complete description of the anisotropy than previous OAF measurements.

In this paper, we discuss at length the results from the analysis of a single TRISO particle, where the optical resolution was ~4 μm. While the TRISO particle chosen for this analysis was fabricated using a set of baseline conditions designed to produce particles with optimal performance, the present analysis shows only an example of the results obtainable using the 2-MGEM technique. (We have analyzed several hundred TRISO particles in this manner.) For this particular TRISO particle, we can conclude:

1. The diattenuation of the IPyC and OPyC layers is considerably higher than the buffer and SiC layers, but the diattenuation in these layers is not uniform. There are regions within each of these layers where the diattenuation is extremely small, and regions where it is significantly greater than the mean. The standard deviation of the distribution is considerably larger than the average error in the diattenuation, making this variation statistically significant.
2. The 2-MGEM measurement also determines the direction of the principal axis at each measured spot, which can be associated with the average direction of the graphene planes. For the IPyC and OPyC layers, this direction is well-defined and lies perpendicular to the radius of the TRISO particle, while there is little or no preferential direction of the buffer and SiC layers. A small value of the standard deviation of the relative principal axis angle SD(γ_r) combined with a large value of the diattenuation corresponds to significant graphene plane organization.

Acknowledgements

Research was sponsored in part by the Office of Nuclear Energy, Science and Technology and Oak Ridge National Laboratory, managed by UT-Battelle, LLC, for the US Department of Energy under Contract No. DE-ACO5-00OR22725.

References

[1] R.W. WyckoffCrystal Structures, vol. 1, John Wiley, 1963, p. 26.
[2] G.E. Bacon, J. Appl. Chem. 6 (1956) 477.
[3] J.C. Bokros, Carbon 3 (1965) 167.
[4] K. Bongartz, Nucl. Technol. 35 (1977) 379.
[5] P.A. Tempest, Carbon 16 (1978) 171.
[6] D.W. Stevens, Carbon 15 (1977) 421.
[7] S. Ergun, Nature 213 (1967) 135.
[8] G.E. Jellison Jr., J.D. Hunn, R.A. Lowden, J. Nucl. Mater. 352 (2006) 6.
[9] G.E. Jellison Jr., D.E. Holcomb, J.D. Hunn, C.M. Rouleau, G.W. Wright, Appl. Surf. Sci. 253 (2006) 47.
[10] D.W. Stevens, Surf. Sci. 96 (1980) 174.
[11] D.W. Stevens, Report to the Department of Energy, GA document A15291, UC-77 (1979).
[12] G.E. Jellison Jr., J.D. Hunn, C.M. Rouleau, Appl. Opt. 45 (2006) 5479.
[13] G.E. Jellison Jr., F.A. Modine, Appl. Opt. 36 (1997) 8184.
[14] G.E. Jellison Jr., F.A. Modine, Appl. Opt. 36 (1997) 8190.
[15] D. Hélary, X. Bourrat, O. Dugne, G. Maveyraud, M. Pérez, P. Guillermier, in: Second International Topical Meeting on High Temperature Reactor Technology, Beijing, China, September 22–24, 2004, paper B07.
[16] E. Pollmann, J. Pelissier, C.S. Yust, J.L. Kaye, Nuc. Tech. 35 (1977) 301.
[17] R.A. Lowden, J.D. Hunn, S.D. Nunn, A.K. Kercher, J.R. Price, P.A. Menchhofer, G.E. Jellison Jr., Effects of deposition conditions on the properties of pyrolytic carbon deposited in a fluidized bed, ORNL/TM-2005/533.